JPMTR 072 | 1435
DOI 10.14622/JPMTR-1435
UDC 655.1 – 024.25 : 621.38

Research paper
Received: 2014-09-01
Accepted: 2015-09-24

Self-supported printed multi-layer capacitors

Michael James Joyce, Ali Eshkeiti, Paul D. Fleming III, Alexandra Pekarovicova and Massood Zandi Atashbar

Western Michigan University,
Center for the Advancement of Printed Electronics (CAPE),
4601 Campus Drive, Room A217,
Kalamazoo MI, 49008

E-mails: Michael.Joyce@wmich.edu,
Ali.Eshkeiti@wmich.edu
Dan.Fleming@wmich.edu
A.Pekarovicova@wmich.edu
Massood.Atashbar@wmich.edu

Abstract

The increasing demand for miniaturized electronic devices has elevated the need for rechargeable micro-power sources. While lithium and lithium ion batteries have been utilized in these applications since the late 1990s, other energy harvesting technologies, such as mechanical, thermal and solar, are now being used to augment batteries to enable systems to be self-powered. However, the lifetime of any battery is finite, which may be a major problem when the application is in a permanent structure or medical implant device. For power or significant energy storage applications, printed multilayer capacitors or supercapacitors are being explored as an enhancement, or replacement of micro-batteries.

The printing of multilayer capacitors offers an inexpensive manufacturing process for these devices. Though the ability to print supercapacitor electrodes, supercapacitors, and batteries on rigid and flexible substrates is well known, having a device supported by a substrate is not always advantageous. This is especially true for cases where the rigidity of the substrate limits the extent to which the device can be bent or wound, or where substrate compatibility issues to the surface to which it is to be attached is faced. The ability to bend or wind devices can improve the attachment to surfaces; enable its placement in confined spaces and advance efforts to further miniaturize devices. In this research, a sacrificial water-soluble polymer layer was used to produce self-supported (substrate free) printed conductive and dielectric ink films of different thicknesses, as well as a completed capacitor. The electrical and mechanical properties of these films and the capacitor were measured. Such measurements have not yet been reported and should therefore advance our understanding of properties at different thicknesses.

Keywords: supercapacitor, printed electronics, screen printing, alginate, silver electrode

1. Overview

The increasing demand for miniaturized electronic devices has grown the need for rechargeable micro-power sources. Though lithium and lithium ion batteries have been utilized in these applications since the late 1990s, other energy harvesting technologies such as thermal, mechanical and solar, are now being used (Pech et al., 2010). The benefit of using energy harvesting technologies to recharge batteries is that they enable systems to be self-powered. However, the useful life of a battery is limited, which may be a serious problem when placed in a permanent structure, such as a concrete support structure, engine or biomedical implant (Kang, 2006). Batteries also cannot provide the peak power for some portable electronic devices without increasing the bulkiness or weight of the device. With developing electronic markets searching for thinner, lighter weight, lower cost and more conformable solutions, printed electronics offers a possible solution to meeting these goals, but a complementary energy source to batteries is still missing (Kaempgen et al., 2009). Electronic capacitors are used to provide charge storage. Their ability to endure millions of cycles and fast charge/discharge rates enables energy densities to be maintained for the balancing of circuitry in electronic devices (Miller and Simon, 2008; Simon and Gogotsi, 2008). For power or significant energy storage applications, multilayer capacitors or supercapacitors can be used to enhance battery performance, which would help batteries fill current and future energy needs (Kaempgen et al., 2009).

The printing of multilayer capacitors offers an inexpensive manufacturing process for producing such devices and the ability to print supercapacitor electrodes, supercapacitors, and batteries are well documented (Simon and Gogotsi, 2008; Kaempgen et al., 2009; Kiebele and Gruner, 2007; Grande et al., 2012). However, everything reported to date has involved the printing of various functional inks on rigid or flexible substrates. The type of

substrate used is often dictated by the processing temperature requirements of the functional materials printed and flexibility requirements of the end product. This study focused on the fabrication and testing of self-supporting printed multilayer capacitors. The roughness, flexibility and density of the printed layers were characterized. A completed capacitor, consisting of four alternating layers of silver and dielectric, was printed and tested. The capacitor was also wound to demonstrate the feasibility of producing a multi-stacked capacitor. The benefits of this research include defining the design and commercial potential for self-supported printed energy storage devices, and advancing the technical knowledge for self-supported printed electronic devices. The findings of this study should also greatly advance work being performed in printed sensors and active transistor devices.

2. Introduction

2.1 Capacitor and supercapacitor technologies

The direct printing of passive (electrodes, resistors, capacitors) and active (thin film transistors, photovoltaics, organic light emitting diodes) devices has gained significant attention as a low cost manufacturing method for flexible electronics. As the global need for energy continues to rise, the risk of facing a supply imbalance also grows. Concerns on how the world will keep pace with growing energy demands have led to increased efforts to find new technologies for harvesting and storing energy. Some of the energy harvesting technologies being explored are light, human movement, vibration and heat, based on technologies such as photovoltaics (Swanson, 2009), electrodynamics (Sterken et al., 2007), and piezoelectronics (Challa et al., 2008).

The harvesting of renewable energy offers just one part of the needed solution. Once harvested, efficient technologies to store the energy are required. Batteries are the most predominant technology used (Linden, 1984), but other technologies such as eutectic systems (Smith and Hashemi, 2006) or mechanical methods, such as flywheel (Ruddell, 2003) and hydroelectric storage (Jog, 1989) can be used.

The two most significant criteria for the performance of an electrical energy storage device are power and energy density. Power density is a measure of how fast energy can be transferred per unit mass into a device ($J \cdot (kg \cdot s)^{-1}$). Energy density is the amount of energy stored per unit mass ($J \cdot kg^{-1}$). Both of these criteria are especially important when device portability is needed (Jiang, 2007).

Two major types of energy storage devices are batteries and capacitors. Batteries directly convert chemical energy to electrical energy through the generation of charge from redox reactions that take place at the electrodes of the battery. The generated charge creates a voltage between the battery's cell terminals. The concentration and chemical species within the battery determines the voltage output. In contrast, capacitors store energy by charge separation. A basic capacitor consists of a dielectric material sandwiched between two parallel electrodes capable of establishing an electrical potential. The dielectric material can be either an ionic solution (electrolyte) or solid material. When a closed circuit between the two electrodes is formed the electrical potential is released generating a power density (Bird, 2010). The two main functions of a capacitor are to charge or discharge electricity and to block the flow of direct current (DC). The function of charging or discharging energy is used in smoothing the circuits of power supplies and backing-up circuits of microcomputers. The function of blocking DC flow enables them to be used as filters to block undesirable frequencies in a circuit. In general, capacitors do not efficiently utilize the material from which they are fabricated so their energy densities are typically low (Bird, 2010).

Electrolytic capacitors evolved from the basic capacitor design. They are similar to batteries, but have an anode and cathode composed of the same materials. There are aluminum, tantalum and ceramic capacitors (Jayalakshmi and Balasubramanian, 2008).

The next evolution in capacitor technology was the creation of electric double layer capacitors, EDLCs, which store electrical charge at a metal/electrolyte interface. The main component of these devices is activated carbon, which is used in the electrode construction of these capacitors. This technology served the needs of industry for many years, then experienced resurgence as interests in electrical storage technology for medical devices, miniature electronic devices and applications requiring very short high power pulsed devices. EDLCs complement batteries by supplying a high power density and low energy density when needed, while lasting longer than batteries. In comparison to conventional capacitors, they have higher energy densities. The disadvantage to EDLCs is that they suffer from low energy density. To address these problems, researchers have explored mixing transition metal oxides with the activated carbon used as the electrode material. This mixing enhanced the specific capacitance by a factor of 10–100, depending on the type of metal oxide used (Halper and Ellenbogen, 2006). The increased performance brought about by this technology introduced a new class of capacitors called supercapacitors or pseudocapacitors.

Supercapacitors have been the focus of much research over more than past 10 years (Butler, Miller, and Taylor,

2002). The difference in performance between a supercapacitor and capacitor can be seen through a comparison of the specific power and specific energy rates as shown in Figure 1.

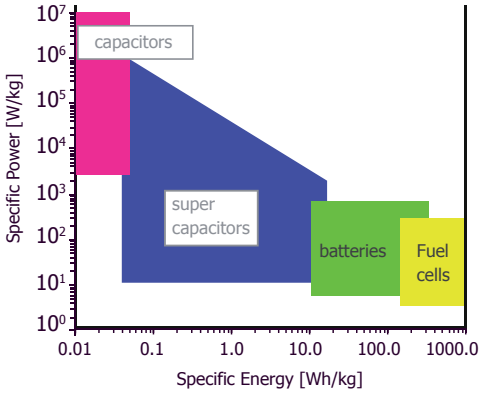

Figure 1: Comparison of different storage devices, modified from Winter and Brodd (2004)

The general equations for capacitance, Equation [1], and energy storage, Equation [2], were first proposed by Helmholtz (1853):

$$C = (A\varepsilon_0\varepsilon)/d \quad [1]$$

$$E = \tfrac{1}{2}CV^2 \quad [2]$$

where C is capacitance (F), E is the energy stored (J or Ws), ε_0 is the permittivity of free space, equaling $8.8541 \cdot 10^{-12}$ F/m, ε is the relative permittivity of the dielectric layer, or dielectric constant, A is the total surface area of the electrodes (m^2), d is the distance between the two parallel electrodes (m), V is the established potential between the electrodes (V).

From Equation [1], it is clear that to achieve very high supercapacitor performance, a combination of maximizing the plate area, minimizing the distance between plates and selecting a dielectric material to maximize the effective permittivity is needed. For printed capacitors, the distance between plates is limited by the thickness of the printed dielectric layer, which is often determined by the printing method used. The permittivity is based on the properties of the dielectric material, which can be deposited/printed, or the original substrate itself. Using a number of geometric techniques, such as stacking alternating plates or winding up a flat device, can result in a flexible capacitor, which can effectively manipulate the area.

By combining these equations from above, the peak energy density per unit mass can be written as Equation [3]:

$$Energy\ Density = E\varrho = (\varepsilon_0/2)(A/d)(\varepsilon V_b^2\varrho) \quad [3]$$

where ϱ is the device density and V_b is the breakdown voltage of the dielectric material. V_b is used instead of V in order to allow the properties of different dielectric materials to be compared.

A close examination of Equation [3] shows three parts: a constant term ($\varepsilon_0/2$), a geometrical term (A/d) and a materials property term ($\varepsilon V_b^2\varrho$). Hence, the energy density of a capacitor can be achieved by altering the geometry and properties of the materials used (Pollet, Marinel and Desgardin, 2004).

The most sophisticated types of ultracapacitors are electrochemical capacitors, ECCs, and electric/electrochemical double layer capacitors, EDLCs. Both devices have capacitance values that are orders of magnitude higher than traditional capacitors, hence, the prefixes super and ultra. An ECC consists of two electrodes immersed in an ionic solution, which enables the accumulation of charge at the double layer interface. The most common uses of ECCs are in hybrid electrical vehicles and in solar and wind power facilities where they are used to supply intermittent energy. EDLCs store charge from ions supplied from an electrolytic solution in contact with high surface area electrodes, typically made from activated carbon. These unique properties enable them to fill the gap between batteries and conventional capacitors.

Both ECC and EDLC technologies are commercially available. The main use of EDLCs are in applications where energy conservation, electrical power load leveling, and high power millisecond long pulse delivery is needed, for example to start an engine or automotive braking system (Jayalakshmi and Balasubramanian, 2008).

The basic differences between the design and construction of two types of ultracapacitors are shown in Figure 2.

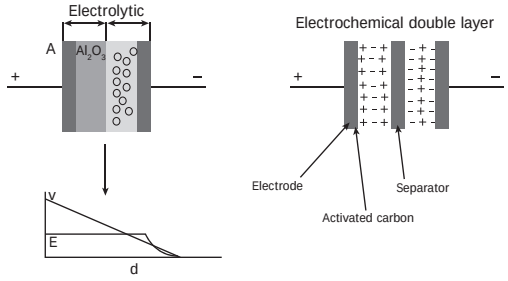

Figure 2: Schematic presentation of electrolytic capacitor and electrical double layer capacitor, recreated from Jayalakshmi and Balasubramanian (2008)

Two other types of capacitors are ceramic and film capacitors. Ceramic capacitors are constructed from alternating layers of metal and ceramic, with the ceramic serving as the dielectric. Multilayer ceramic capacitors (MLCs) typically contain around 100 alternating layers encased in two ceramic layers. They are fabricated by

screen-printing both the conductive and dielectric layers, and subsequently, co-sintering them together. The most commonly used material for the conductive (electrodes) and dielectric layers is Ag-Pd and $BaTiO_3$, respectively (Pollet, Marinel and Desgardin, 2004).

Since the year 2000, when the communications market began to flourish, the demand for MLCs has increased to keep pace. Other ceramic materials that have been identified are $CaZrO_3$, $MgTiO_3$, and $SrTiO_3$. Mn and Ca are some of the other electrode materials being used. Film capacitors, just as the name suggests, are made using thin films of polyester or polypropylene. These materials are used with the dielectric and meta-glazed capacitors, which consist of Al electrodes created by the vapor deposition of Al onto a polyester, polypropylene, or polycarbonate film (Nagata et al., 2006; Keskinen et al., 2012).

Recent printed electronics research has examined nano-gold, graphene, nano-silver, nano-copper, single-wall and multi-wall carbon nanotubes (CNT) as electrode materials (Grande et al., 2012; Keskinen et al., 2012; Le et al., 2011; Hartman, 2011). A comparison of a few different conductive inks for use in printed electronics is shown in Table 1.

In addition to the conductive inks listed above, graphene has also been heavily studied as a conductive material for pseudocapacitors. Graphene is a non-toxic nano-material, which is readily dispersible; it is the most conductive form of carbon. It does not require high temperature sintering and therefore can be used with plastic film and paper substrates. It also gives the ability to be deposited as very thin layers, and is less expensive than silver, copper, and CNT inks.

A comprehensive review of recent research performed using graphene in energy harvesting/storage devices and printed electronics was recently performed by Grande et al. (2012) and Nair et al. (2008), showed graphene to be a feasible alternative to indium tin oxide (ITO) in OPVs, due to the ability of a single layer of graphene to transmit 98 % of total incident light. Blake et al. (2008), reported films of graphene having a sheet resistivity of approximately 6 kΩ/sq. This corresponds to a bulk resistivity of about $2 \cdot 10^{-6}$ Ωm. The sheet resistance of graphene was found to depend on the quality of the graphene sheets. The fewer the defects in the sheets, the lower the sheet resistance. Several reports have also shown the method of synthesis greatly impacts the sheet resistance of graphene.

The use of graphene to produce supercapacitors with specific energy densities comparable to Ni metal hydride batteries for hybrid vehicles was recently demonstrated by Liu et al. (2010). The supercapacitors produced have the advantage of being rechargeable in less than 2 minutes, which is faster than what can be obtained with current hybrid battery technologies. Wang et al. (2009) and Yu, Davies and Chen (2010) synthesized 25 nm thick graphene/graphite sheets using a vacuum filtration method, which enabled a capacitance of 135 F/g to be realized. The graphene sheets produced by this method were found to be flexible and transparent, thus capable of being used in applications where transparent supercapacitors would be needed.

The use of hybrid CNT/graphene composites in polyethyleneimine (PEI) and polyaniline (PANI) in supercapacitors was explored by Yu, Davies and Chen (2010) and Wang et al. (2009), respectively. Capacitances of 120 F/g and 210 F/g, respectively, at a current density of 0.3 A/g were achieved. Han, Ding and Shang (2010) used polypyrrole (PPy) and obtained a capacitance of 223 F/g at a current density of 0.5 A/g. PPy has the advantage of being more stable under ambient conditions in comparison to PANI.

Jari et al. (2012) explored the use of graphene to create supercapacitors. In their work, supercapacitor electrodes of 2 cm^2 and 0.5 cm^2 using activated carbon were prepared. They showed standard 2 cm^2 capacitors to have typical capacitance values of 30–35 F/g with only the activated carbon mass taken into account. They also compared electrodes printed from 3 commercial silver inks to graphene electrodes and found no practical differences in their conductivity values with typical sheet resistances of 0.03–0.05 Ω/sq for 20–30 μm thick layers (Keskinen et al., 2012).

Graphene oxide (GO) has also been studied. Although, alone it is not electrically conductive, the addition of thermal, chemical, and photothermal processes reduces

Table 1: Comparison of conductive inks for PE applications (Grande et al., 2012)

Ink	Conductivity	Oxide	Film cohesion	Process concerns
Silver	Excellent	Conductive	Good	Long drying times
Carbon	Average	Does not form	Poor	None
Copper	Good	Non-conductive	Good	Ink stability
Polymer	Average	Does not form	Good	Low solubility
CNT	Excellent	Does not form	Poor	Toxic

it to graphene. A recent study by Le et al. (2011) showed the ability to inkjet print a mass fraction of 0.2 % water based GO ink with a viscosity of 1.06 mPa·s and surface tension of 68 mN/m on a Dimatix inkjet printer. Once printed, GO electrodes were thermally reduced under N_2 atmosphere at 200 °C to graphene. Even though these ink characteristics were outside the recommended ranges for normal inkjet printing (i.e., 10–12 mPa·s and 28–32 mN/m), Le et al. (2011) found that by manipulating the firing voltages of the nozzles as a function of time spherical ink droplets without clogging could be produced. A spatial resolution of ~ 50 μm was achieved. Titanium foils from Sigma Aldrich (100 μm thick, 99.99 % purity) were used as a comparison for electrochemical performance. The use of two identical electrodes clamped with a Celgard separator produced a specific capacitance of 48–132 F/g in the scan range of 0.5 to 0.01 V/s for the graphene electrodes, and were able to retain 96.8 % of the capacitance over 1 000 cycles. It was also shown that graphene electrodes prepared by conventional powder based methods were similar in performance to the inkjet printed electrodes (Wu et al., 2010).

Although graphene and carbon nanotube inks are good alternative electrode materials to silver, the printing of these nano-materials can be difficult. The difficulty in printing these materials is due to their hydrophobic nature, which causes them to segregate in water, unless surfactants are added, or their surfaces are functionalized (Le et al., 2011).

Silver inks, on the other hand, are well established in the market place. Inkjet, screen, flexo, and gravure Ag inks are readily available and have been used as electrode materials in many printed electronics applications. Solvent based silver inks are of special interest to this study, due to their high water resistance, which is required to allow for lifting off the printed layer through the use of a sacrificial water-soluble base layer.

Printed supercapacitors need to be flexible and capable of being printed or attached onto multiple substrates. To be useful, the performance of the storage device should meet the life expectancy of the product. Low cost and ease of production would increase their acceptance. Printed energy sources that could be integrated into a printed device in line would greatly reduce the fixed production costs of supercapacitor systems.

2.2 Lift-off processes

Several methods for the lift-off of printed electronic devices have been reported (Ogier, Veres and Yeates, 2003; Greer and Howard Jr., 1989; Haskal, McCulloch and Broer, 2010; Rogers et al., 2010). Ogier, Veres and Yeates (2003) describe the use of a lift-off ink to enable the printing and lift-off of organic electronic devices, mainly organic light emitting displays, OLEDs. The lift-off ink is printed as a negative image and then sequential device layers are printed on top. To lift-off the device, a lift-off solution, which dissolves the lift-off ink, but not the device layers, is applied. The process requires the use of ultrasonic agitation, stirring, a spray liquid medium and/or heat to be used. Haskal, McCulloch and Broer (2010) describe a laser lift-off process that uses the wet casting of a plastic coating, containing a UV absorbing additive, to a substrate followed by the screen or inkjet printing of thin film electronic elements to fabricate an active display matrix. The laser is used to lift-off the plastic layer after it has been printed from the carrier substrate. Greer and Howard Jr. (1989) describe a lift-off process to remove any unwanted areas from a metallization layer to form a layer of masking material over a semiconductor device. Lift-off occurs upon heating of the device to a temperature where the metal melts on the masking layer and forms globules when it cools, which can be removed. Rogers et al. (2010) described a carrier layer coated with a sacrificial layer to which a stretchable substrate is attached. The stretchable substrate is printed with electronic devices, and removed to produce a self-supporting stretchable device. This process can presumably make strain-independent electronic devices (Rogers et al., 2010).

This study focused on the feasibility of screen-printing a self-supported capacitor. The capacitor was fabricated using a commercially available solvent-based silver and UV dielectric ink. Information on the conductive (silver), and dielectric (acrylate) inks is listed in Table 2.

The novelty of this work is that a newly discovered lift-off process was used for the first time to obtain a self-supported capacitor. The work demonstrates that a self-supported fully printed capacitor could be wound, resulting in multi-stacked conductive and dielectric layers. The findings suggest that it may be possible to create a supercapacitor by winding a self-supporteddielectric-conductive-dielectric-conductive printed stack.

Table 2: Commercial inks used

Supplier	**Ink type**	**Commercial name**
Sun Chemical	Thermal flake silver	AST 6200
Henkel	UV dielectric	Electrodag PF-455B

3. Experimental methods

3.1 Creation of sacrificial layer

A water-soluble solution of sodium alginate was applied to sheets of Melinex ST 506 PET film (DuPont, Chester, VA) using different Byrd applicators to obtain films of different thicknesses. The alginate (S-160-QD, SNP Inc., Durham NC) was applied to the PET as a 6 % aqueous solution. Alginate solutions were prepared by slowly sprinkling the appropriate amount of dried alginate into a pre-weighted amount of deionized water under agitation. Once all alginate was added, the solution was allowed to mix for 60 minutes to ensure complete hydration. The solution was then placed in a closed container in a refrigerator overnight to enable it to degas. After 24 hours, the solution was removed and brought to room temperature, approximately 21 °C, before applying it to the PET film. The PET film was cleaned with isopropyl alcohol just prior to application of the alginate solution. While preparing the alginate films of different thickness from the 6 % solution, it was observed that during drying the alginate films were cracking. To alleviate this problem, glycerol was added to the solution of alginate to help plasticize the film. The addition level of glycerol that was found to give the most uniform alginate film was a mass fraction of 20 % of dry alginate. From this solution, films were then prepared using #0.5, 1.0, 6.0, 8.0 and 10 mil Byrd applicators. Unfortunately, these films were very thin and could not be easily removed and handled. To create films that could be more readily handled Meyer rods were used instead. After experimenting with several different rods, #14 and #20 rods were chosen. The films produced using these rods were strong enough to handle without tearing, and readily dissolved in water when rewetted. The thicknesses of these films were found to be 6.88 and 14.41 μm, respectively.

After coating, the samples were placed in a conditioned room at 50 % RH and 23 °C (allowing for reproducible and consistent drying conditions). The roughness (S_a) and thicknesses of the films were then measured with a Bruker GT-K white light interferometer microscope at a magnification of 50× giving a sample area of approximately 0.125 mm × 0.098 mm. Three measurements were taken on each film sample prepared (for both roughness and thickness). Two films for each condition were tested. After the initial roughness measurements were obtained, it was apparent that the amount of particulate matter in the air throughout the building and within the conditioning room was significant, so handling procedures were adjusted to minimize contamination. All coated samples were placed in an enclosed ("clean") environmental chamber to dry, and kept in closed containers during transport to and from the print stations and drying/curing stations. The environmental chamber used was a Carron RH chamber maintained at a temperature of approximately 21 °C and 50 % RH for 24 hours. Drying refers to the thermal treatment of the applied silver ink, while curing refers to the UV treatment of the dielectric ink. The thermal treatment of the silver ink is required to evaporate the solvents allowing the silver particles to create a more intimate, uniform, and continuous layer. The UV treatment is used to initiate and propagate a polymerization reaction, which in turn forms the "dried" dielectric film.

After characterizing the properties of the alginate films, single and multilayer prints were prepared according to Figure 3. The two different thicknesses of alginate and ink layers are denoted by the +1 and −1 conditions as shown and explained in the figure caption. Ink films of different thicknesses were obtained by printing single and double layers of the ink. The ink films were dried/cured in between prints, allowing for measurements to be taken. Samples were prepared in this way to allow for the characterization of the alginate films and single layer prints alone, before characterizing the multilayer prints. This methodology also allowed the impact of each layer on the final device performance to be better understood.

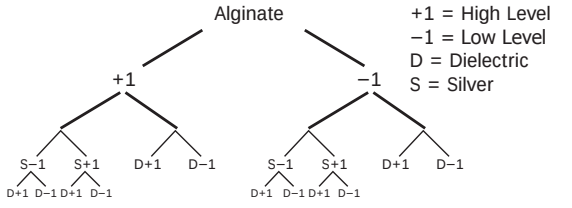

Figure 3: Sequence of sample preparation: −1 for alginate obtained using a #14 Meyer rod and +1 obtained using a #20 Meyer rod, S−1 and D−1 refer to single layer silver and dielectric, and S+1 and D+1 refer to double layer silver and dielectric, respectively

3.2 Printing

The print pattern used is shown in Figure 4. Figure 4a shows each individual layer and how they were overlaid onto one another, while Figure 4b depicts the completed final device.

The inks were screen-printed onto the alginate coated PET samples using an AMI MSP-485 semi-automated screen printer. Double layer samples were accomplished by first printing and drying/curing the first layer prior to printing the second layer on top of the first. The samples were then cured/dried using a Fusion UV curing unit equipped with a D bulb (Peak Radiated Power at approximately 375 nm, FusionUV, 2015). The samples were passed through the Fusion UV curing unit at 75 m/min, until fully cured (no longer tacky to the touch), which took anywhere from 3 to 4 passes. Using an IR tempera-

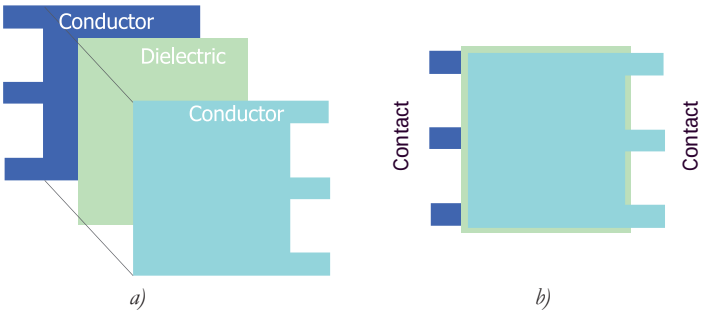

Figure 4: Three layer structure in a) exploded view, b) top view

ture probe, the curing unit temperature within the Fusion UV drier was measured to be 54.4 °C, which was sufficient to fully dry the silver ink after 3–4 passes. The pattern printed for each ink was a 5 cm × 5 cm solid block. The specifications for the screen used are given in Table 3. After drying/curing, the roughness (S_a) and thickness of the printed films were measured.

Table 3: Screen specifications

Manufacturer	Specifications
Microscreen (South Bend, IN)	230 lpi mesh 0.0011" wire diameter at 45° wire angle 10 μm thick emulsion

3.3 Removal of the sacrificial layer

After measuring all the desired properties of the PET printed samples, the samples were wetted with room temperature (21 °C) deionized (DI) water to dissolve the sacrificial layer of sodium alginate and the printed layers lifted-off the PET. After retrieving the self-supported films from the water, the films were blotted dry and retained for further measurement.

3.4 Characterization of film properties

The Young (1805) equation has been known for over two centuries. Its modified form (Equation [4]) is as follows:

$$\gamma_{LV}\cos\theta = \gamma_{SV} - \gamma_{SL} \qquad [4]$$

where γ_{LV} is the liquid-vapor interfacial tension or surface energy, γ_{SV} is the solid-vapor interfacial tension, γ_{SL} is the solid-liquid interfacial tension, and θ is the contact angle.

This equation and the measured value of the contact angle are still being used as the basis for calculating the surface free energies of the films. However since its inception, as the result of further studies, other contact angle measurement methods for the determination of the surface free energy of polymeric materials have evolved. These methods have been widely adopted as they are relatively easy to perform and of high accuracy. One such method is the Owens–Wendt method. In this method, the surface free energy of a solid is determined from the following Equation [5]:

$$\sqrt{\gamma_S^d \gamma_L^d} + \sqrt{\gamma_S^p \gamma_L^p} = 0.5\gamma_L\left(1+\cos\theta\right) \qquad [5]$$

where γ_S^d, γ_L^d, γ_S^p, γ_L^p are dispersion and polar components and γ_L is the surface free energy of measuring liquid. Because γ_S^d and γ_L^p are both unknowns, this equation is insufficient to determine the surface free energy of a solid. Thus, the contact angle of two liquids of known surface tension must be measured. By making these measurements, two linear equations in the form below, with different values of the constant coefficients are obtained (equations [6a] and [6b]).

$$x + ay = b\left(1+\cos\theta_1\right) \qquad [6a]$$

$$x + cy = d\left(1+\cos\theta_2\right) \qquad [6b]$$

where $x = \sqrt{\gamma_S^d}$, $y = \sqrt{\gamma_S^p}$, and θ_1 and θ_2 are the contact angle values of the two known liquids, and a, b, c, d are the coefficients dependent on the kind of liquids used. For this method, one liquid with a dominant polar component and one liquid with a dominant dispersive component should be used. By using such liquids, the solution of the system of above linear equations is affected as little as possible by the errors accompanying the determination of the γ_L^d and γ_L^p values.

The Owens-Wendt method is one of the most common methods used for calculating the surface free energy of solids and the two most frequently used measurement fluids used are water and methylene iodide (diiodomethane). This method was used to determine the surface energies of the films. The contact angles of water and methylene iodide were measured with a First Ten Ångstrom dynamic contact angle measurement device, which captures the change in contact angle with time with a high-speed video camera (FTA, 2015; Owens and Wendt, 1969). Once captured, the change in contact angle with time was plotted, and the equilibrium contact

angle obtained and used in the calculation of the surface energy of the solid to which the liquids were applied. Five equilibrium contact angles were obtained for each fluid from which five surface free energy values were calculated. The equilibrium contact angle is the angle where no further change in contact angle with time was observed. The average surface free energies (total, polar and dispersive) for each sample are reported.

The resistance of the conductive ink layers and capacitance (using the dielectric ink films as the insulating layer with dielectric test fixture) were measured with the instruments listed in Table 4. The dielectric constant of the dielectric layers was then calculated from the capacitance measurements using Equation [1]. The sheet resistivities of the samples were obtained using a four point probe sensing station consisting of a Keithley 2602 Dual Source Meter with a SMR Probe Head from Bridge Technology. The two outer probes are used for sourcing the current, and the two inner probes are used for measuring the voltage across the layer. The sheet resistivity is calculated from the measured voltage, applied source current, and dimensions of the conducting layer. After printing all the layers of the capacitors, the capacitance was measured using an LCR meter (Agilent E4980A) over a range of frequencies (1 Hz to 1 MHz), and the impedance response was measured. Based on the response, the capacitance values were calculated. Attempts to measure the electrical properties while being flexed on a Mark-10 instrument and attached to a Keithley 2602 Dual Source Meter failed, due to the inability of the samples to survive the test without tearing. To determine the densities of the films, the weights, thicknesses, and areas of the printed free films were measured. The areas were measured using an ImageXpert image analyzer. The weights were obtained using a Mettler digital balance. Attempts to determine the stiffness of the films with a Gurley Stiffness test instrument failed due to the stiffness of the films being below the detectable limits of the instrument.

Table 4: Electrical characterization equipment and measurement parameters

Test Equipment	**Measurement Parameters**
Keithley 4200-SCS Semiconductor Characterization System	Capacitance (for final device only), Resistance, Effective Dielectric Constant
Keithley 2602 Dual Source Meter	1 Ω to 1 MΩ Surface Resistance
Keithley 6517A High Impedance Test Set and ASTM D257 Resistivity Test Fixture	> 1 MΩ Surface Resistance
Agilent 4338B mΩ Meter	< 1 Ω Surface and Bulk Resistance
Agilent E4980A LCR Meter	Capacitance (for final device only), Effective Dielectric Constant

4. Results

The surface free energies of the alginate coated PET films are shown in Table 5. As shown, the surface free energy increased with increasing film thickness. This could be because at the higher alginate film thickness, the lower surface free energy PET did not influence the measurement, but for the thinner alginate film, it did. This is reasonable explanation when one considers the high solubility of alginate in water. It should be noted that observations were made, after running the test, showing less of the thinner alginate film remained on the area where the water made contact in comparison to the thicker alginate film (testing took approximately 30 seconds).

The high surface free energy of the alginate film is due to the large number of carboxyl and hydroxyl groups in the polymer (Figure 5) (visit-alginate, 2015). The polar groups attract the polar components of the test

Table 5: Influence of alginate film thickness on surface free energy

Substrate (Alginate Film Thickness)	**PET**	**+1* (14.41 µm)**	**−1* (6.88 µm)**
Polar [mJ · m^{-2}]	2.3 ± 0.2	30.3 ± 0.2	15.5 ± 0.2
Dispersive [mJ · m^{-2}]	41.5 ± 0.2	29.7 ± 0.5	31.3 ± 0.5
Surface free energy [mJ · m^{-2}] (polar + dispersive)	43.8 ± 0.5	60.0 ± 0.7	46.8 ± 0.7

*Refer to Figure 3

fluid (i.e., water, H_2O), pulling the fluid's molecules away from one another and toward those contained on the substrate causing the fluid to spread. This increased spreading then lowers the contact angle at which the fluid contacts the substrate's surface decreasing the fluid's thickness (e.g. water, ink, etc.).

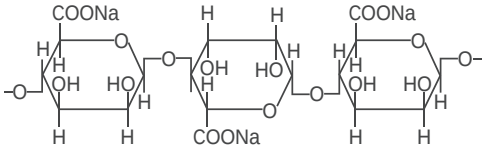

Figure 5: Molecular structure of sodium alginate (FP-Chem, 2011)

The surface roughnesses of the +1 and −1 alginate films (which are the 14.41 and 6.88 μm thick alginate films, respectively) are shown in Figure 6. The average roughnesses, S_a, of the +1 and −1 films are 0.44 and 0.28 μm, respectively. The higher roughness of the thicker alginate film could be the result of the coarser grooves on the #20 Meyer rod or greater film shrinkage.

After fully characterizing the alginate layers, the roughness and thickness of the dielectric and conductive layers printed over the alginate films, according to the experimental setup, were measured. The results are shown in Figures 7 and 8.

The roughness values of the silver layers were significantly higher than the dielectric layers due to the presence of silver flakes in this ink. The roughness of the alginate layers had little or no effect on the roughness of either the conductive or dielectric layers. This would indicate that the thickness of these layers, as a result of the properties of the ink, screen-printing or drying processes, was sufficient to overcome the roughness of the alginate film. Since the roughness of the alginate film was related to its thickness, it can be concluded that the thickness of the alginate film had no influence on the roughness of the printed layers.

A comparison of the 14.41 μm (+1) and 6.88 μm (−1) alginate printed samples shows an influence of these layers on ink film thickness of both the single and double layer printed conductive and dielectric ink films. All

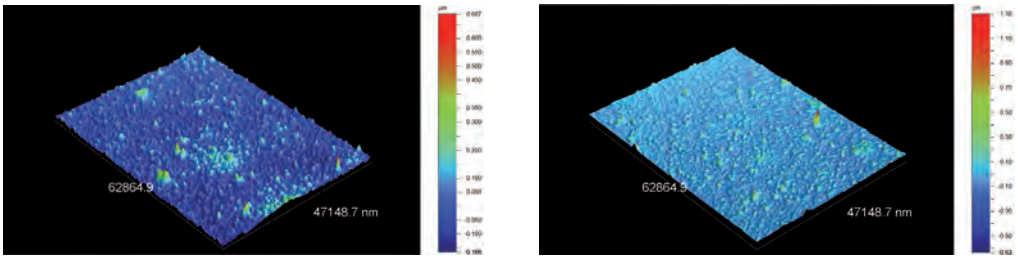

a) *b)*

Figure 6: Surface roughness a) of the +1 (14.41 μm) alginate film, b) of the −1 (6.88 μm) alginate film

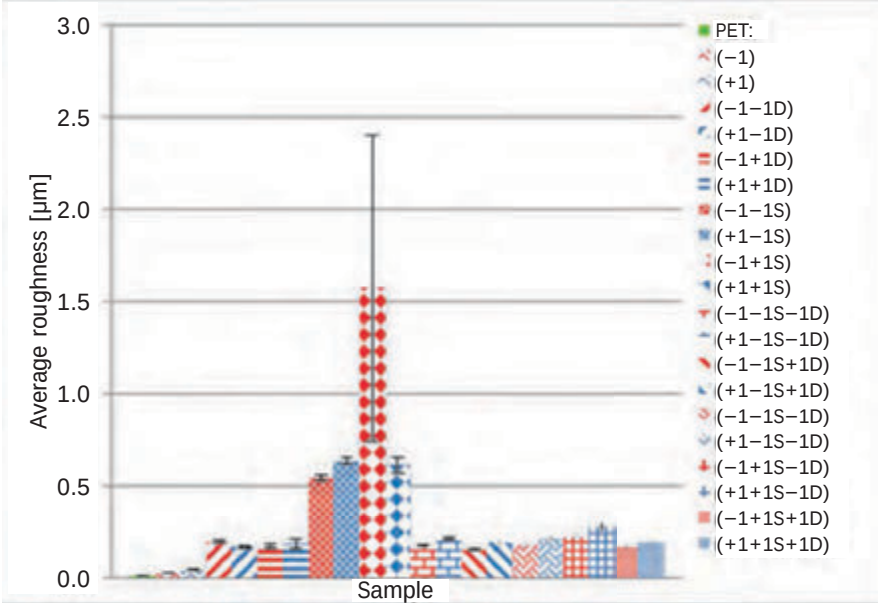

Figure 7: Variations in alginate and ink film roughness with printed and coated layer thicknesses

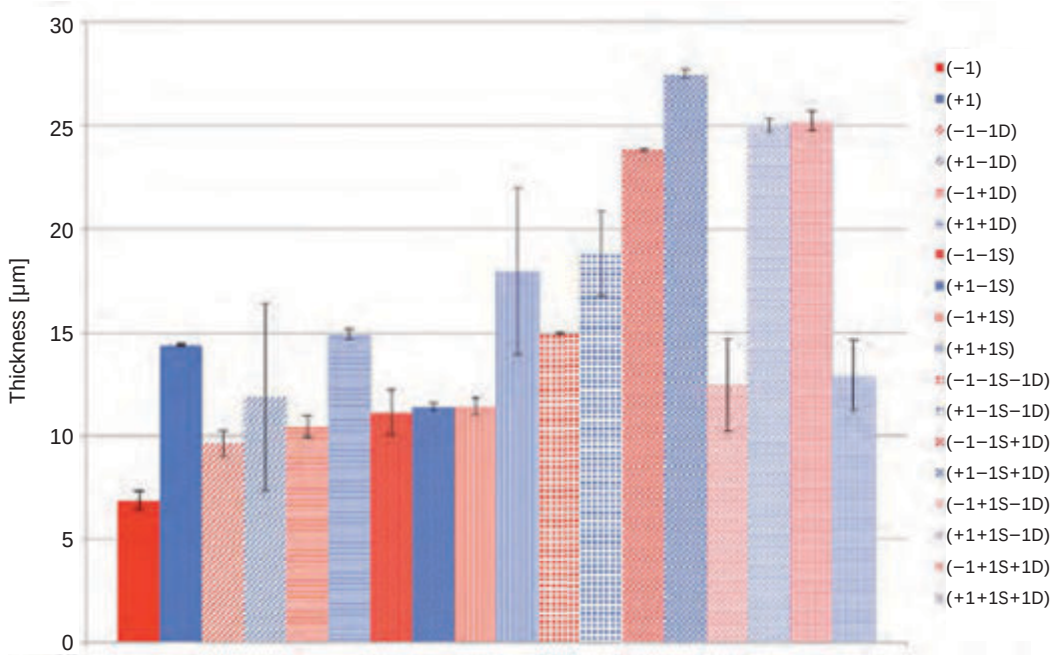

Figure 8: Comparison of film thickness values

dielectric ink films (single and double, −1D and +1D respectively) were thinner than the conductive ink films. It is also seen that all ink films printed on the 6.88 µm (−1) alginate films are thinner in comparison to the 14.41 µm (+1) films, with the exception of the (+1−1S−1D) sample. This could be attributed to the differences in surface free energies of the alginate films. The higher polarity (due to the presence of carboxyl and hydroxyl groups on the alginate, Figure 5) of the 14.41 µm (+1) alginate film could prevent the dielectric and conductive inks from spreading, consequently producing a thicker ink film.

Due to edge effects, the thicknesses of the single and multilayer films were difficult to measure. Edge effects are common with all printed samples, due to ink spreading. The contact angle is a measure of liquid wetting and spreading, the lower the contact angle, the more liquid (ink) wetting that occurs. The amount of spreading that occurs can also be influenced by how quickly the ink film is dried. Since the samples were printed on film, spreading would be expected to be greater, than if printed on a porous substrate. As shown in Figures 9 and 10, the thicknesses of the printed layers were lower at the edges, where more spreading occurred. This can be seen in both the 2D topographical image in Figure 9, and from the representative topographical profile of the x-profile in Figure 10, where the slope of the line decreases from left to right. The high magnification of the Bruker GT-K objective (only a 50× objective was available for use) also increased the difficulty of this measurement by minimizing the area of view to approximately 0.125 mm × 0.09 mm.

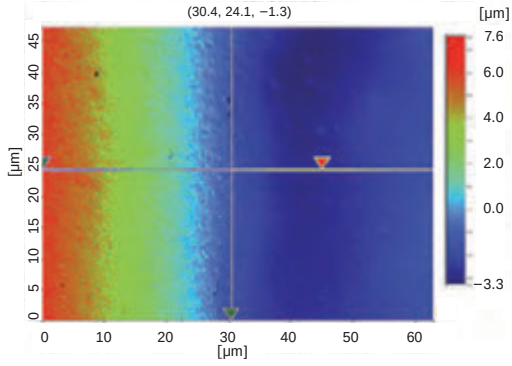

Figure 9: Topographical image of −1D ink on +1 alginate edge effect

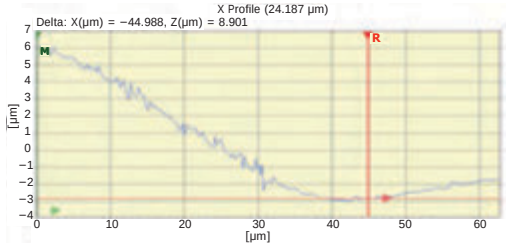

Figure 10: Profile of −1D ink on +1 alginate edge effect

The sheet resistivities of the conductive printed layers are shown in Figure 11. All measurements were made on PET. Figure 11 shows the importance of reporting sheet resistivity versus alginate layer thickness. The large deviations show the unreliability of this test method. The bulk resistivities of the samples are shown in

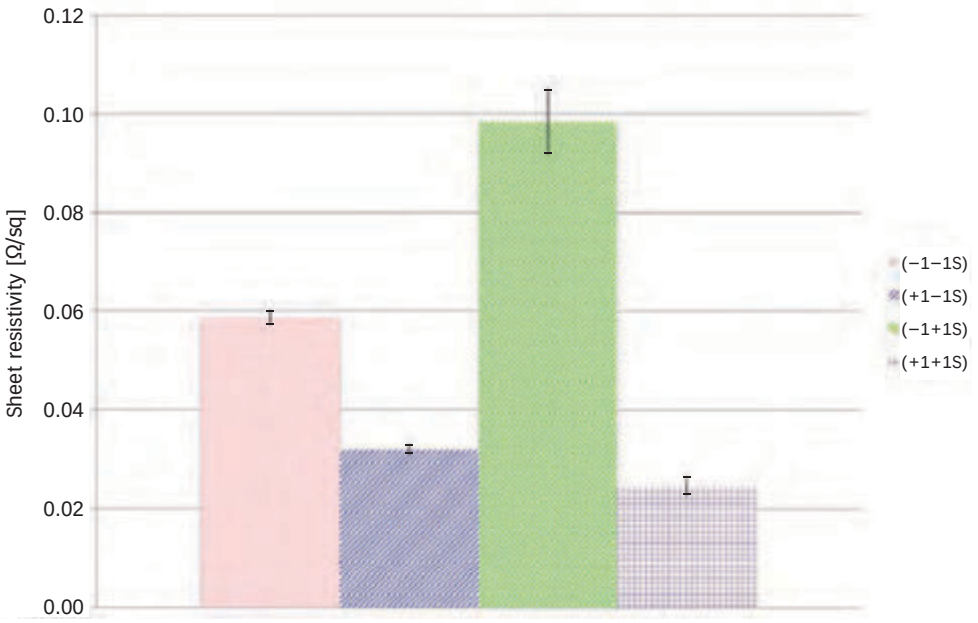

Figure 11: Changes in sheet resistivity of single and double printed silver ink layers as a result of altering the thickness of the sacrificial alginate coating layer

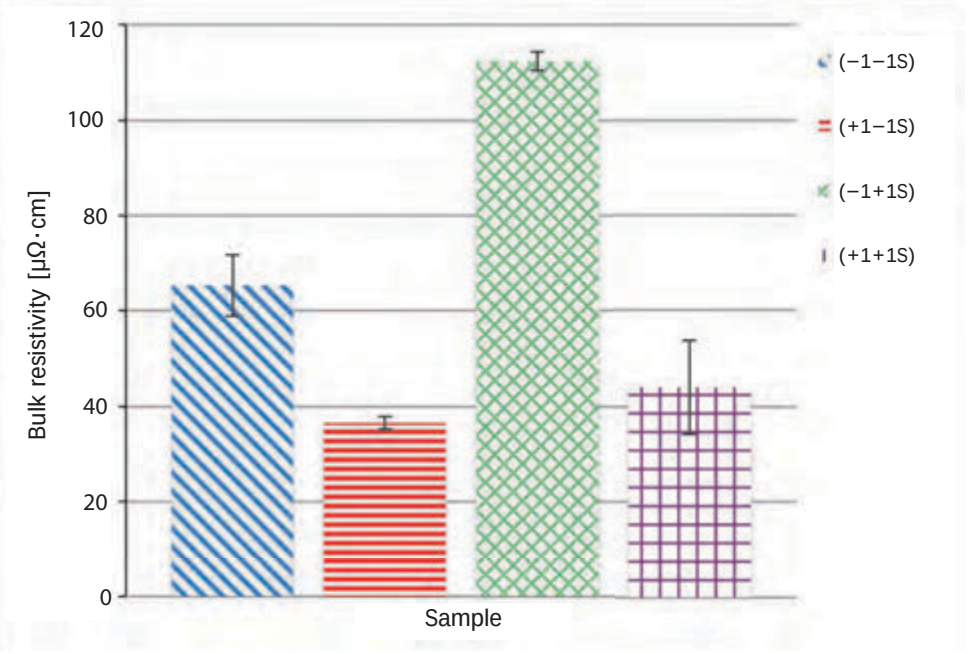

Figure 12: Changes in bulk resistivity of single and double printed silver ink layers as a result of altering the thickness of the sacrificial alginate coating layer

Figure 12. Bulk resistivity (e.g., units Ω · cm) accounts for the thickness of the ink film within its calculation, while sheet resistance does not. It does this by multiplying the sheet resistance by the thickness, giving a resistance times length. The performances of the thicker ink films are significantly better due to the additional thickness. For this reason, the sheet resistivities of the double layer conductive samples are lower than the single layer samples. The thickness of the alginate layer had a greater effect on the sheet resistivity of the thinner conductive film in comparison to the thicker one.

As seen in Figure 13, the dielectric constants are lower for the ink films lifted-off the thinner alginate coated

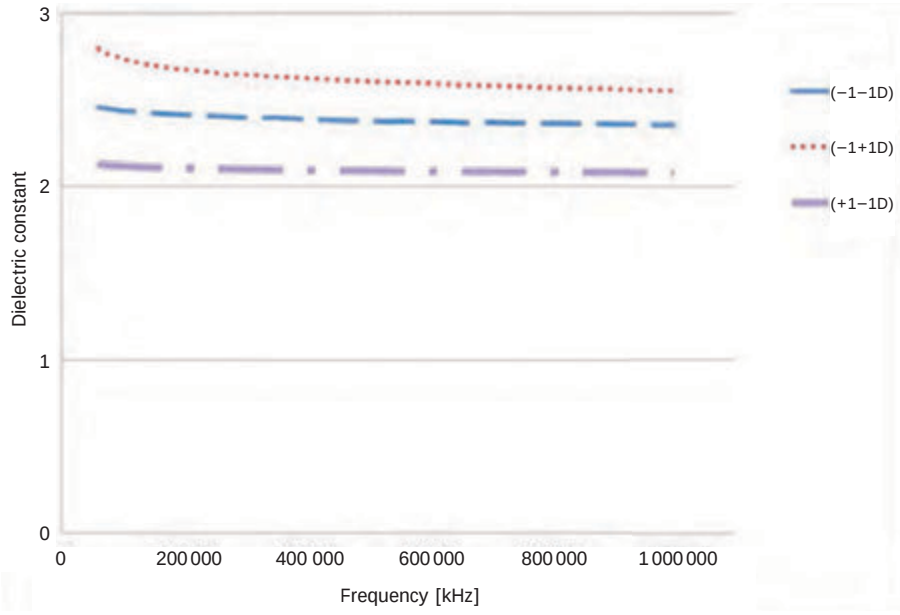

Figure 13: Comparison of the dielectric constants of single and double layer printed dielectric ink layers over alginate films of varying thicknesses

PET samples in comparison to the dielectric film printed on the thicker alginate sample. The +1+1D sample was not reported because its values were repeatedly measured as being negative, indicating that the thickness values for these samples were wrong. Unfortunately, the measurements could not be repeated without reprinting all the samples for consistency of the results.

Ink film densities were able to be determined after removal of the films from the PET. Figure 14 shows the results obtained by measuring the weight and caliper of the samples of known dimensions. From Figure 14 it may be seen that the density of the second layer is higher than that of the first layer (for both the silver and dielectric inks). This could be due to an incomplete removal of solvents in the first layer, or due to inaccuracies of the thickness measurements incurred by the edging effects. By having solvent left in the first layer prior to drying of the second layer the second layer during curing acts as a solvent trap on the solvents trying to escape from the first layer. If the same percentage of solvent was removed, all the silver films would have the same density and all the dielectric films would have the same density.

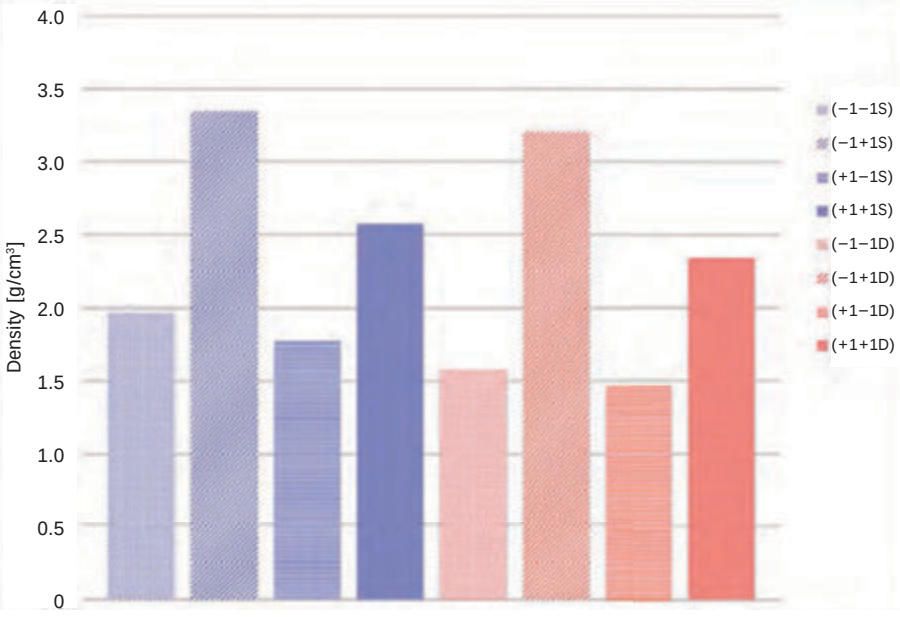

Figure 14: Changes in ink film density resulting from the printing of a second silver and dielectric layer

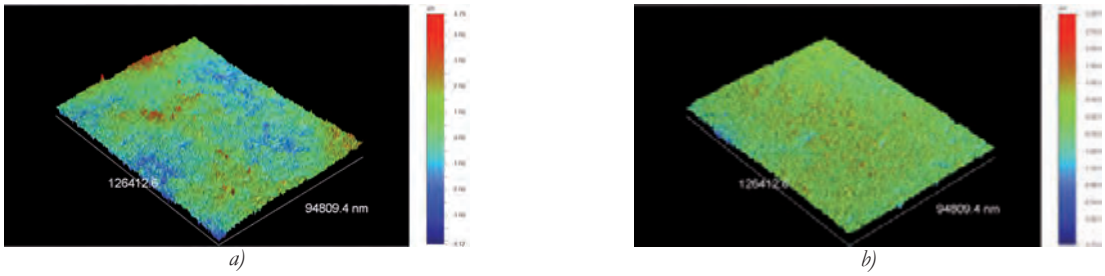

a) *b)*

Figure 15: Roughness of the self-supported ink films for a) −1+1S top side (S_a = 0.74 µm), b) −1+1S bottom side (S_a = 0.342 µm)

In Figure 15 the top and bottom side roughness of the self-supported conductive (silver) ink films are compared (these are free films, no substrate supporting them). As shown, the roughness of the topside (the side that was not in contact with the PET film) is nearly twice as rough as the side of the film, which was in direct contact with the alginate coated PET film prior to its removal in water.

Similar differences can be seen between the top side and bottom side for all the silver films in Figure 16.

The difference in surface topography of the top and bottom surface of the films is attributed to the difference in the smoothness of the surfaces in which they are in contact. That is, the top side is the side that contacts the printing screen, which is highly rough due to the mesh openings, as well as being exposed to the particulate matter within the environment during drying. In opposite, the bottom side of the ink film is in direct contact with the highly smooth (in relation to the printing screen) alginate coated PET film, and is protected from the environment during drying. This difference in roughness is apparent when looking at the differences between the top and bottom S_a statistical values. The S_a value depicts the average roughness averaged over an area (a 3D parameter) (Olympus-IMS, 2015; Cohen, 2013). The differences in topography of the top and bottom side of the conductive ink films shows an approximate 50 % reduction in S_a values.

One of the main objectives of this research was to determine if the self-supported films (combined to create a capacitor) could be wound without damage to the ink layers and capacitor itself. This objective was successfully achieved. A single stacked, self-supported capacitor was successfully created as seen in Figure 17, and successfully wound without damage, as seen in Figure 18. The gain in device flexibility as a result of not having a carrier substrate layer is obvious. These encouraging results show promise for the use of this technology as a means to produce a supercapacitor by winding a multi-stacked device or to minimize the size of a device to fit into tight places or where substrate compatibility issues to the surface to which it is to be attached is faced. The ability to bend devices can improve the attachment to surfaces, enabling its placement in confined spaces and advancing efforts to further miniaturize devices. It has also been shown that

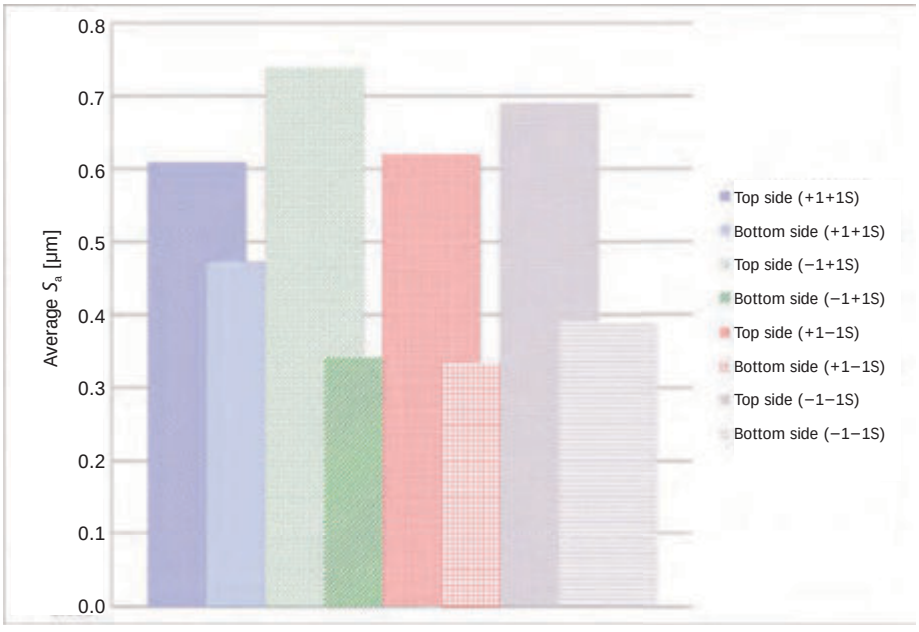

Figure 16: Comparison of top side and bottom side roughness of self-supported single layer silver ink films

the side of the printed film lifted off the rigid substrate is much smoother. This can be advantageous for multi-layer prints by requiring less ink to achieve complete surface coverage. So in practice, a printed film could be lifted from a smooth surface, flipped, and printed with minimal ink for coverage. By demonstrating that the self-supported layers could be rolled, it is feasible that a supercapacitor could be created through the addition of an insulating layer to prevent shorting upon winding. This work is currently in progress.

Figure 17: Self-supported unwound capacitor

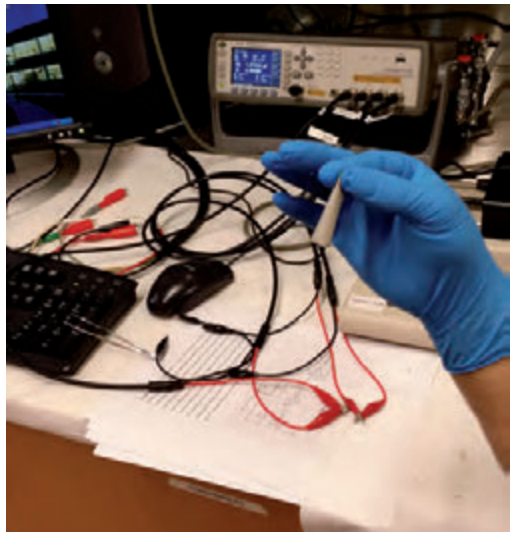

Figure 18: Self-supported wound capacitor

5. Conclusions

A process to produce self-supported electrically functional ink layers was demonstrated. Smooth alginate films on a PET substrate (sacrificial substrates) were produced by coating a 6 % solution of alginate with a mass fraction of 20 % of glycerol. This film served as a sacrificial layer for enabling the lift-off of screen-printed thermal conductive and UV dielectric ink films from a PET film after immersion of the printed samples in distilled water. The thickness of the alginate film was found to influence the thickness of the printed dielectric and conductive layers, which impacted their electrical performance. The ability to produce self-supported films to determine the dielectric constant of a dielectric ink film at different thicknesses was demonstrated. This is further supported by the fact that the final dielectric measurement of 3.81 (dielectric constant), calculated (using Equation [1]) from the final capacitance measurements (from the fully printed capacitor) was within range of what the manufacturer (Table 2) reported (which is about 4). This was also true for the conductive inks' sheet resistivity measurements, which were reported as being between 0.015–0.020 Ω/sq. The finding of the differences from the top to bottom side conductive film roughness is of great interest. The ability to use the bottom side of a printed layer, for use when high smoothness is required may prove to be valuable. The density measurements also proved to be highly useful when calculating for the bulk resistivity and will be highly useful for any situation where accurate densities need to be accomplished. The ability to wind a fully printed self-supported capacitor was demonstrated and holds promise for the creation of supercapacitors by this technique.

References

Bird, J., 2010. *Electrical and Electronic Principles and Technology,* New York: Routledge.

Blake, P., Brimicombe, P.D., Nair, R.R., Booth, T.J., Jiang, D., Schedin, F., Ponomarenko, L.A., Morozov, S.V., Gleeson, H.F., Hill, E.W., Geim, A.K. and Novoselov, K.S., 2008. Graphene-based liquid crystal device. *Nano Letters,* 8(6), pp. 1704–1708.

Butler, P., Miller, J.L. and Taylor, P.A., 2002. *Energy Storage Opportunities analysis: Phase II Final Report, A Study for the DOE Energy Storage Systems Program.* Albuquerque, New Mexico, Sandia National Laboratories.

Challa, V.R., Prasad, M.G., Shi, Y. and Fisher, F.T., 2008. A vibration energy harvesting device with bidirectional resonance frequency tenability. *Smart Materials and Structure,* 17(1), pp. 1–10.

Cohen, D.K., 2013. *The connection between surface texture and sliding friction*. [online] Available at: <https://www.bruker.com/fileadmin/user_upload/8-PDF-Docs/SurfaceAnalysis/AFM/Webinars/Bruker-SlidingFriction-presentation-07262013.pdf> [Accessed 16 August 2015].

FP-Chem, 2011. *Sodium Alginate*. [online]. Available at: <http://www.fp-chem.com/index.php?c=msg&id=373&> [Accessed 17 August 2015].

FTA, 2015. *Owens-Wendt Surface Energy Calculation*. [online] Available at: <http://www.firsttenangstroms.com/pdfdocs/OwensWendtSurfaceEnergyCalculation.pdf> [Accessed 16 August 2015].

FusionUV, 2015. *An Electrodeless Bulb for Consistency and Long Life* [online]. Available at: <http://www.fusionuv.com/uv_bulbs.aspx> [Accessed 16 August 2015].

Grande, L., Chundi, V.T., Wei, D., Bower, C., Andrew, P. and Ryhänen, T., 2012. Graphene for Energy Harvesting/Storage Devices and Printed Electronics. *Particuology,* 10(1), pp. 1–8.

Greer, S.E. and Howard Jr., R.T., 1989. *Lift-off process for terminal metals*. U.S. Pat. 4,861.425.

Halper, M.S. and Ellenbogen, J.C., 2006. *Supercapacitors: A Brief Overview*. MITRE Nanosystems Group, MITRE Corporation, McLean, Virginia, USA.

Han, Y., Ding, B. and Shang, X., 2010. Preparation of graphene/polypropyrole composites for electrochemical capacitors. *Journal of New Materials for Electrochemical Systems,* 13(4), pp. 315–320.

Hartman, A., 2011. *Printing Carbon Nanotube Based Supercapacitors for Packaging*. Master thesis, Clemson University.

Haskal, E.I., McCulloch, D.J. and Broer, D.J., 2010. *Active matrix displays and other electronic devices having plastic substrates*. U.S. Pat. 2010/0163,878.

Helmholtz, H.v., 1853. Über einige Gesetze der Vertheilung elektrischer Ströme in körperlichen Leitern mit Anwendung auf die thierisch-elektrischen Versuche. *Annalen der Physik und Chemie,* 89(6), pp. 211–233.

Jayalakshmi, M. and Balasubramanian, K., 2008. Simple capacitors to supercapacitors – an overview. *International Journal of Electrochemical Science,* 3, pp. 1196–1217.

Jiang, Z., 2007. *Technology Assessment and Market Analysis of Solid State Ultracapacitors*. Master thesis, Massachusetts Institute of Technology.

Jog, M.G., 1989. *Hydroelectric and Pumped Storage Plants*. New Delhi: New Age International.

Kaempgen, M., Chan, C.K., Ma, J., Cui, Y. and Gruner, G., 2009. Printable thin film supercapacitors using single-walled carbon nanotubes. *Nano Letters,* 9(5) pp. 1872–1876.

Kang, J.Y., 2006. Micropower for Medical Application. In: J.G., Webster, ed., *Encyclopedia of Medical devices and Instrumentation*. New Jersey: Wiley-Interscience.

Keskinen, J., Sivonen, E., Jussila, S., Bergelin, M., Johansson, M., Vaari, A. and Smolander, M., 2012. Printed Supercapacitors on Paperboard Substrate. *Electrochimica Acta,* 85, pp. 302–306.

Kiebele, A. and Gruner, G., 2007. Carbon nanotube based battery architecture. *Applied Physics Letters* 91(14), p. 144104.

Kinaret, J., Falko, V., Ferrari, A., Helman, A., Kivioja, J., Neumaier, D., Novoselov, K., Palermo, V. and Roche, S., 2012. *Coordination Action for Graphene-Driven Revolutions in ICT and Beyond*. Graphene Flagship: Deliverable 6.3 "Publishable flagship proposal report", EC grant nº284558.

Le, L.T., Ervin, M.H., Qiu, H., Fuchs, B.E., Zunino, J., and Lee, W.Y., 2011. Inkjet-printed graphene for flexible micro-supercapacitors. In: *11th International Conference on Nanotechnology*. Portland, Oregon, USA.

Linden, D., 1984. *Handbook of batteries and fuel cells*. New-York: McGraw-Hill.

Liu, C., Yu, Z., Neff, D., Zhamu, A. and Jang, B.Z., 2010. Graphene-based supercapacitor with an ultrahigh energy density. *Nano Letters,* 10(12), pp. 4863–4868.

Miller, J. R. and Simon, P., 2008. Electrochemical capacitors for energy management. *Science,* 321(5889), pp. 651–652.

Nagata, H., Ko, S.W., Hong, E., Randall, C.A., Trolier-McKinstry, S., Pinceloup, P., Skamser, D., Randall, M. and Tajuddin, A., 2006. Microcontact printed $BaTiO_3$ and $LaNiO_3$ thin films for capacitors. *Journal of the American Ceramic Society,* 89(9), pp. 2816–2821.

Nair, R.R., Blake, P., Grigorenko, A.N., Novoselov, K.S., Booth, T.J., Stauber, T., Peres. N.M.R. and Geim, A.K., 2008. Fine structure constant defines visual transparency of graphene. *Science,* 320(1308), p. 1308.

Ogier, S.D., Veres, J. and Yeates, S.G., 2003. *Organic electronic devices,* EP 1529317 A2.

Olympus-IMS. 2015. *Roughness (3D) parameter*. [online] Available at: <http://www.olympus-ims.com/en/knowledge/metrology/roughness/3d_parameter/> [Accessed 16 August 2015].

Owens, D.K. and Wendt, R.C., 1969. Estimation of surface free energy of polymers. *Journal of Applied Polymer Science,* 13(8), pp. 1741–1747.

Pech, D., Brunet, M., Taberna, P.L., Simon, P., Fabre, N., Mesnilgrente, F., Conédéra, V. and Durou, H., 2010. Elaboration of a microstructured inkjet-printed carbon electrochemical capacitor. *Journal of Power Sources*, 195(4), pp. 1266–1269.

Pollet, M., Marinel, S. and Desgardin, G., 2004. $CaZrO_3$, a Ni-co-sinterable dielectric material for base metal-multilayer ceramic capacitor applications. *Journal of the European Ceramic Society,* 24, pp. 119–127.

Rogers, J.A., Huang, Y., Ko, H.C., Stoykovich, M., Choi, W.M., Song, J., Ahn, J.H. and Kim, D.H., 2010. *Stretchable and foldable electronic devices*. U.S. Pat. 2010/0002402.

Ruddell, A. 2003. *Investigation on Storage Technologies for Intermittent Renewable Energies: Evaluation and recommended R&D strategy*. Storage Technology Report: WP-ST6: Flywheel.

Simon, P. and Gogotsi, Y., 2008. Materials for electrochemical capacitors. *Nature Materials,* 7(11), pp. 845–854.

Smith, W.F. and Hashemi, J., 2006. *Foundations of materials science and engineering*, Boston: McGraw-Hill.

Sterken, T., Fiorini, P., Van Hof, C. and Puers, R., 2007. A Hybrid Electrodynamic Vibration Harvester. In: *Proceedings of Power MEMS 2007*, pp. 85–88.

Swanson, R.M., 2009. Photovoltaics Power Up. *Science,* 324(5929), pp. 891–892.

visit-alginate, 2015. [online] Available at: <http://www.visit-alginate.com/sodium-alginate-chemical-properties.html> [Accessed 16 August 2015].

Wang, Y., Shi, Z., Huang, Y., Ma, Y., Wang, C., Chen, M. and Chen, Y., 2009. Supercapacitor devices based on graphene materials. *The Journal of Physical Chemistry C,* 113(30), pp. 13103–13107.

Winter, M. and Brodd, R.J., 2004. What are batteries, fuel cells, and supercapacitors? *Chemical Reviews,* 104(10), pp. 4245–4270.

Wu, Q., Xu, Y., Yao, Z., Liu, A. and Shi, G., 2010. Supercapacitors based on flexible graphene/polyaniline nanofiber composite films. *ACS Nano,* 4(4), pp. 1963–1970.

Young, T., 1805. An essay on the cohesion of fluids. *Philosophical Transactions of the Royal Society of London,* 95, pp. 65–87.

Yu, A., Roes, I., Davies, A. and Chen, Z., 2010. Ultrathin, transparent, and flexible graphene films for supercapacitor application. *Applied Physics Letters,* 96(25), p. 253105.